http://dx.doi.org/doi:10.2174/22117385113019990002

Poly(allylamine) Magnetomicelles for Image Guided Drug Delivery

Christopher M Barnett[1], Martin R Lees[2], Anthony DM Curtis[3], Paul Kong Thoo Lin[4], Woei Ping Cheng[5], Clare Hoskins[6]*

1. Barnett CM, School of Pharmacy, Keele University, Keele, ST5 5BG, UK
2. Lees MR, Physics Department, University of Warwick, Coventry, CV4 7AL, UK
3. Curtis ADM, Institute for Science and Technology in Medicine, School of Pharmacy, Keele University, Keele, ST5 5BG, UK
4. Kong Thoo Lin P, School of Life Sciences and Pharmacy, Robert Gordon University, Aberdeen, AB24 1HG, UK
5. Cheng WP, School of Pharmacy, University of Hertfordshire, Hatfield, AL10 9AB, UK
6. Hoskins C*, Institute for Science and Technology in Medicine, School of Pharmacy, Keele University, Keele, ST5 5BG, UK

*Corresponding author: Tel. +441782 734799, Fax: +441782 733326, Email: c.hoskins@keele.ac.uk

Abstract

Polymeric micelles have received considerable interest for their use as drug delivery vehicles for hydrophobic drug solubilisation. Inorganic metallic nanoparticles have already been exploited clinically in diagnostics for their contrast ability, using magnetic resonance imaging. The combination of these two platforms results in a multifunctional drug carrier for image-guided drug delivery. Here we report the synthesis and evaluation of a new class of poly(allylamine) (PAA) polymer grafted with hydrophobic oxadiazole (Ox) pendant group in a 5% molar monomer:pendant ratio. Further, the thiol-containing pendant group facilitated the attachment of hybrid iron oxide-gold nanoparticles (HNPs) *via* dative covalent bonding. Physicochemical characterisation of both PAA-Ox_5 and PAA-Ox_5-HNP polymers was carried out using elemental analysis, nuclear magnetic resonance (NMR), fourier transform infrared spectroscopy (FTIR) and photon correlation spectroscopy (PCS). The drug loading potential of these novel aggregates was investigated, through direct conjugation of hydrophilic and encapsulation of hydrophobic drugs, respectively. The model hydrophobic drugs 2,6-diisopropylphenol (propofol) and (2S,6'R)-7-chloro-2',4,6-trimethoxy-6'-methyl-3H,4'H-spiro[1-benzofuran-2,1'-cyclohex[2]ene]-3,4'-dione (griseofulvin), and the chemotherapeutic agents bisnapthalamidopropyldiaminooctane (BNIPDaoct) and 6-Thioguanine (6-TG) were used. The data showed that the addition of HNPs onto the PAA-Ox_5 structure resulted in aggregates of 175 nm in diameter. The PAA-Ox_5-HNP nano-aggregates were capable of high drug solubilisation capacities (25.79 $mgmL^{-1}$, 1.68 $mgmL^{-1}$ and 0.92 $mgmL^{-1}$) for propofol, griseofulvin and BNIPDaoct, respectively. 6-TG was also successfully conjugated into the polymer structure (2.8 $mgmL^{-1}$). *In vitro* assays on human pancreatic adenocarcinoma cells (BxPC-3) showed increased drug uptake and decreased IC_{50} values using the novel formulations compared with free drug. This study highlights the potential of PAA-Ox_5-HNP as a bi-functional imaging and drug delivery platform.

Keywords: Magnetomicelle, amphiphilic polymer, hybrid nanoparticle, drug solubilisation, image guided drug delivery

Introduction

Polymeric amphiphiles have proven to be an excellent alternative to low molecular weight surfactants for drug solubilisation [1-3]. In aqueous environments, they spontaneously aggregate into micelle-like aggregates *via* hydrophobic-hydrophobic interactions [4]. Polymeric nano-aggregates can be formed from a diverse range of architectures including block copolymers [5], graft polymers [6], star shaped polymers [7] and dendrimers [8]. Graft polymers consist of a water-soluble homopolymer backbone with hydrophobic groups 'grafted' onto this to form a comb shaped structure [9]. Commonly, poly(ethylenimine) [10], poly(allylamine) [11] and chitosan [12] backbones have been used in the formation of these macromolecules. Previous work has reported the promising potential of poly(allylamine) (PAA) grafted with cholesteryl and dansyl moieties to act as universal hydrophobic drug solubilizers [13]. Model drugs included 2,6-diisopropylphenol (propofol), 11β-11,17,21-trihydroxypregna-1,4-diene-3,20-dione (prednisolone) and (2S,6'R)-7-chloro-2',4,6-trimethoxy-6'-methyl-3H,4'H-spiro[1-benzofuran-2,1'-cyclohex[2]ene]-3,4'-dione (griseofulvin) [13].

In recent years, magnetic iron oxide nanoparticles have been widely studied for biomedical and electronic applications. These applications include: detection at the cellular level, imaging using nuclear magnetic resonance imaging (MRI), targeted drug delivery and gene therapy, waste water treatment and electronics [14-18]. Iron oxide nanoparticles possess a large surface area to volume ratio due to their nano-size, a low surface charge at physiological pH and they also aggregate in solution due to their inherent magnetic properties. The subsequent stability problems in solution can be overcome by surface engineering of the particles with coatings such as silica and polymers [14,19]. However, in the last few years, increasing concern has arisen over the safety of polymer coated iron oxide nanoparticles [20-22]. This culminated in the withdrawal of Feridex® from use in humans in the United Kingdom in 2012. It is proposed that the degradation of the flexible polymer coating leads to iron oxide core exposure, resulting in free radical production and, ultimately, cellular stress or mortality [21,23,24]. The need for a robust coating has therefore led to the recent development of gold-iron oxide hybrid nanoparticles (HNPs) [25]. Gold is renowned for its chemical stability and biocompatibility in the nano-shell structure [26]. Gold nanostructures can be further functionalised using molecules that possess a thiol group which are strongly adsorbed onto the gold surface [27]. Previous studies investigating HNP fabrication have shown that the insertion of an organic intermediate between the iron oxide core and gold coating helps to preserve the unique characteristics of both the iron oxide and gold components [25,28]. A recent study has also investigated the effect of the hybrid composition on HNP physicochemical properties, i.e., changing the core size, coating thickness *etc.* in order to harvest optimal particles [28]. Additionally, *in vitro* biocompatibility testing has reported no considerable HNP degradation or toxic effect [29]. Thus, indicating the suitability of these HNPs for biomedical application.

The incorporation of polymeric amphiphiles and HNPs into a single platform may therefore create a bi-functional system capable of dual imaging and drug delivery of active pharmaceutical ingredients. In this study we aim to graft water-soluble PAA with 5-(4-chlorophenyl)-1,3,4-oxadiazole-2-thiol (oxadiazole, Ox) in a 5% monomer:pendant group ratio (PAA-Ox_5). The oxadiazole moiety is hydrophobic due to its aromatic structure and also possesses a thiol (SH) functionality. This pendant group will act as a site of permanent conjugation for

the HNPs; achieved through the strong dative covalent attachment between the thiol and colloidal gold surface. The physicochemical properties of the novel PAA-Ox_5 will be investigated both before and after HNP conjugation. The potential of these nano-aggregates as drug cargo carriers in the aqueous environment will also be investigated. The model hydrophobic drugs propofol and griseofulvin will be used to determine optimal drug solubilisation parameters. Propofol is the most commonly used intravenous anaesthetic agent in the world owing to its rapid onset, short half-life and minimal side-effect profile [30]. The highly lipophilic nature of the compound (logP 4.16) hinders its formulation as an aqueous-based injection. Early propofol formulations utilised Cremophor EL (a non-ionic surfactant) in water but were associated with characteristic adverse effects including severe anaphylactic hypersensitivity reactions [31]. Subsequently, propofol was reformulated into a microemulsion formulation (e.g. Diprivan®) which is still the current preparation used clinically [32]. However, some limitations remain, including pain upon injection and support for bacterial growth [33]. Griseofulvin is a lipophilic drug with an aqueous solubility of 30 μgmL^{-1} at 25 ºC [34]. The antifungal properties of griseofulvin are exploited in both animals and humans for the treatment of dermatophyte infections [35,36]. Its hydrophobic nature results in a low aqueous solubility in the gastrointestinal (GI) tract resulting in poor oral bioavailability [37,38]. Griseofulvin is currently administered orally in microcrystalline preparations with prescribed doses of 500-1000 $mgday^{-1}$ [39]. However, a great deal of inter- and intra-subject variation is experienced, perhaps due to erratic and incomplete absorption of the drug from the GI tract [40]. The novel anticancer drug bisnaphthalimidopropyldiaminooctane (BNIPDaoct) has been reported to possess great potential as a cytotoxic agent in pancreatic cancer treatment [41,42]. BNIPDaoct has shown negligible aqueous solubility and as a result toxic solvents such as dimethyl sulfoxide (DMSO) have been required in order to dissolve the drug [41,43]. Here, we will investigate the potential of the two PAA derivatives in BNIPDaoct solubilisation using the optimal formulation strategies determined. Additionally, the potential of these novel nano-aggregates to act as hydrophilic drug carriers will be investigated using 6-thioguanine (6-TG). 6-TG is an antitumour agent used clinically in the treatment of leukaemia [44]. However, its association with a large number of serious side effects such as ulcerative colitis and bone marrow toxicity, has seen its use decline in recent years [45]. 6-TG will be conjugated onto the PAA-Ox_5-HNP surface *via* dative covalent bonding in a similar process to the polymer HNP conjugation. The drug conjugation capacity will be determined using PAA-Ox_5 as a control. *In vitro* studies in human pancreatic adenocarcinoma (BxPC-3) cells will determine the effect of drug incorporation into the PAA amphiphiles on both drug uptake and cytotoxicity.

Materials and Methods

Materials

Poly(allylamine) (PAA), 5-(4-chlorophenyl)-1,3,4-oxadiazole-2-thiol and auric chloride dihydrate were purchased from AlfaAesar (UK). Dialysis tubing membranes were purchased from Medicell International Ltd. (UK). Syringe filters (0.22 µm), acetonitrile, methanol and dimethyl sulfoxide (DMSO) were purchased from Fisher Scientific (UK). Foetal bovine serum, Roswell Park Memorial Institute Medium (RPMI) 1640, trypsin and penicillin streptomycin were purchased from Life Technologies (UK). Human pancreatic adenocarcinoma (BxPC-3) cells were purchased from ATCC (USA). All other chemicals were purchased from Sigma-Aldrich (UK).

Methods

PAA-Ox_5 synthesis

PAA was reacted in 1:0.05 molar feed with 5-(4-chlorophenyl)-1,3,4-oxadiazole-2-thiol (Oxadiazole, Ox) (monomer: pendant). Briefly, the PAA was dissolved in 1:1 (v/v) methanol: chloroform with stirring followed by the addition of triethylamine. The reaction was stirred at room temperature for 0.5 h. The 5-(4-chlorophenyl)-1,3,4-oxadiazole-2-thiol was dissolved in 1:1 (v/v) methanol:chloroform and added drop wise to the polymer solution over 0.5 h. The reaction was stirred at 37°C for 18 h. After evaporating the solvent on a reduced pressure using a rotary evaporator the polymer residue was washed three times with diethyl ether and dried thoroughly. The residue was dissolved in deionised water and exhaustively dialysed using visking membrane 12-14 kDa against deionised water for 24 h. The resultant solution was freeze-dried. Polymer structure was characterised using proton nuclear magnetic spectroscopy (^{1}H NMR, 400MHz at 25^{o}C) in deuterated water (D_2O) (Bruker, UK), attenuated total reflectance-fourier transform infrared spectroscopy (ATR-FTIR) (Nicolette IS50, Thermo-Fisher UK) and elemental analysis on a Perkin Elmer series 2 elemental analyser (Perkin Elmer, UK).

HNP synthesis

Sodium hydroxide (NaOH) and potassium nitrate (KNO_3) were dissolved in deionised water and heated to reflux at 90 ˚C for 1 h under a nitrogen (N_2) atmosphere. Iron (III) sulfate heptahydrate ($FeSO_4.7H_2O$) was dissolved in sulfuric acid (H_2SO_4) and added to the reaction. The reaction was stirred at 90 ˚C for 24 h. The precipitate was cooled and washed in deionised water. A poly(ethylenimine) (PEI) intermediate was attached electrostatically *via* probe sonication with magnetic particles in deionised water. Gold seeds (2 nm) were attached through electrostatic interaction to the polymer followed by iterative reduction of auric chloride dehydrate ($HAuCl_4$) onto the particle surface forming a complete shell. The final particles were washed extensively with deionised water to ensure excess gold was removed from the solution before resuspending in deionised water. Metal content was determined using inductively coupled plasma – optical emission spectroscopy (ICP-OES). An acid digestion was carried out in concentrated nitric acid (HNO_3, 1:5 sample: acid) and the samples were diluted with deionised water prior to analysis. A calibration was run using iron and gold standard solutions 0.5 – 5 mgmL^{-1} (R^2=0.9999). The concentration of HNPs used for all experiments indicates the concentration of Fe. Maximum UV absorbance (λ_{max}) of HNPs was measured using a UV-2600 UV-VIS(NIR) with an ISR-2600 Plus Integrated sphere (Shimadzu, Germany) of samples in aqueous solution. Solutions were analysed in quartz cuvettes, absorbance scans were carried out between 400 – 800 nm. Hydrodynamic diameter and polydispersity index were estimated using photon correlation spectroscopy (PCS) (Zetasizer Nano-ZS, Malvern Instruments, UK). All measurements were carried out at 25 °C (n=3). Zeta potential measurements were carried out to determine surface charge using the same instrument. Transmission electron microscopy (TEM) was used to visualise the morphology and diameter of particles on formvar-coated copper grids using a JEOL JEM-1230 microscope with ANAlysis software (JEOL, Japan). Magnetic characterisation was carried out in a Quantum Design MPMS-XL SQUID magnetometer as previously described [28]. Briefly, zero-field-cooled warming (ZFCW) and field-cooled-warming (FCW) and cooling (FCC) curves were measured between 10 and 280 K, in a field H = 8 kA/m. Magnetisation *vs.* applied field hysteresis loops were collected at 10 and 250 K in applied fields up to 4 MA/m.

PAA-Ox_5-HNP conjugation

A 5 $mgmL^{-1}$ PAA-Ox_5 (10 mL) solution was prepared in deionised water with probe sonication for 10 min. HNPs (500 µL) were added into solution and the mixture was sonicated for a further 10 min.

Characterisation of PAA-Ox_5 and PAA-Ox_5-HNP nano-aggregates

Nano-aggregates were formed in aqueous solution *via* probe sonication. Solutions were filtered using 0.22 µm syringe filters prior to further analysis. The critical aggregation concentration (CAC) was determined using a hydrophobic methyl orange UV probe in an adaptation of Uchegbu's method [46]. Briefly, a stock solution of methyl orange (25 µM) was prepared with sodium tetraborate buffer (0.02 M, pH 9.4) in deionised water. Polymer solutions (0.00145 - 3 $mgmL^{-1}$) were made up using the methyl orange solution as the diluent. Each sample was probe sonicated for 5 min and allowed to cool to room temperature. The polymer solutions were measured in a UV-2600 UV-VIS(NIR) spectrometer (Shimadzu, Germany) and their maximum absorbance recorded (350-600 nm). The methyl orange stock solution was used as the control. The presence of hypsochromic shift was determined by comparing the polymer solution wavelength maxima with the λ_{max} of methyl orange stock solution (463 nm). Photon correlation spectroscopy, zeta potential measurement, TEM imaging and magnetic characterisation was carried out as previously described.

Drug loading of nano-aggregates

Probe sonication was used to incorporate drug molecules into the self-assemblies as previously reported [11,14]. Aqueous polymer solutions (1, 3 and 6 $mgmL^{-1}$) were probe sonicated for 10 min. Hydrophobic drugs (propofol and griseofulvin) were added to solution using initial drug: polymer feed ratios of 1:1, 5:1 and 10:1. The solutions were sonicated for a further 10 min before cooling to room temperature. The solutions were filtered using 0.22 µm syringe filters to remove any excess unsolubilised drug molecules. Anticancer therapeutic agents 6-TG and BNIPDaoct were incorporated into the nano-aggregate structure using the optimal polymer concentration / drug feed ratio determined using the model drug studies.

Propofol, griseofulvin and 6-TG concentration were determined *via* absorbance measurement at 272 nm, 292 nm and 330 nm in the UV-Vis spectrophotometer, respectively. Propofol and griseofulvin measurements were achieved upon sample dilution in acetonitrile and methanol, respectively. 6-TG measurements were carried out in aqueous samples. BNIPDaoct concentration was measured using a JASCO PH-980 coupled with a JASCO FP-920 fluorescent HPLC (JASCO, Japan). A ODS H: Optimal column (Metlab, UK) of 150 mm x 4.6 mm x 5 µm was used with mobile phase consisting of 55:45 (v:v) buffer:acetonitrile. The buffer was composed of 0.46 g octane sulfonic acid and 1.64 g anhydrous sodium acetate made up to 200 mL with deionised water and pH adjusted to pH 4.6. The mobile phase was run at 1 $mLmin^{-1}$ and sample analysis carried out at excitation and emission wavelengths of 234 nm (Ex.) and 394 nm (Em.) respectively. BNIPDaoct measurements were carried out in samples diluted in 50:50 (v:v) DMSO:H_2O. All measurements were carried out at room temperature (25^{o}C) and the drug encapsulation concentrations deduced in respect to calibration graphs. For all formulations the % drug loading capacity (LC) and % drug encapsulation efficiency (EE) were calculated. The optimal

formulations for each drug molecule were analysed using PCS, zeta potential measurement and TEM, as previously described. The formulations were freeze-dried and ATR-FTIR spectra obtained.

In vitro drug release from nano-aggregates

The formulation (2 mL) was pipetted inside dialysis tubing (MW cut off = 12-14 kDa) and dialysed against PBS under '*sink conditions*' (200 mL, 0.2 M) at 37 ºC with stirring. At various time points, 1 mL of the external PBS was extracted and replaced with 1 mL of fresh PBS. The drug concentration in PBS was determined using UV-Vis and fluorescent spectroscopy, as previously described.

Biological characterisation of nano-aggregates and formulations

BxPC-3 cells were maintained using RPMI media supplemented with 10% foetal bovine serum and 1% penicillin streptomycin. Cells were grown in an incubator at 37 °C and 5% CO_2.

The level of cytotoxicity of PAA-Ox_5 and PAA-Ox_5-HNP was determined *via* the 3-[4,5-dimethylthiazol-2-yl]-2,5-diphenyltetrazolium bromide (MTT) assay on BxPC-3 cells over 24 h. Briefly, the cells were seeded into 96-well plates (15,000 cells/well) and incubated with increasing concentration of polymer solutions (0-0.5 $mgmL^{-1}$). The plates were incubated for 24 h before the solutions were removed and cells washed with fresh media. MTT solution (50 µL, 5 $mgmL^{-1}$) was added to the wells and the plate was incubated (37 °C with 5 % CO_2) in the absence of light for 4 h. The MTT solution was removed and the remaining purple formazan complexes dissolved in DMSO (100 µL). The sample absorbance as recorded at 570 nm using a Tecan Pro200 microplate reader (Tecan, UK). Percentage viability was calculated relative to the positive and negative controls (media and Triton-X (1:5 PBS), respectively). Cytotoxicity assays for the anticancer drugs 6-TG and BNIPDaoct alone ($0.5 – 1x10^{-6}$ $mgmL^{-1}$) and the drug formulations in PAA-Ox_5 and PAA-Ox_5-HNP polymers were carried out. Here, polymer concentration of 0.001 $mgmL^{-1}$ was used as this was above the IC_{90} value obtained from the previous study.

Drug uptake studies were carried out after 4 h incubation of the novel formulations of 6-TG and BNIPDaoct. Cells were seeded in a 6-well plate (50,000 cells/well) and incubated with 50 μgmL^{-1} drug concentration (in formulation compared with free drug). Plates were incubated for 4 h at 37 °C, 5% CO_2 before the media was removed and the cells washed three times with phosphate buffered saline (PBS). The cells were trypsinised and resuspended in 1 mL media. Cells were counted on a Countess® automated cell counter (Life Technologies, UK), $1 x10^6$ cells transferred into an Eppendorf tube and centrifuged at 500 rpm for 5 min. The cell pellet was resuspended in deionised water (6-TG)/DMSO (BNIPDaoct) and vortexed for 30 seconds. The sample absorbance was recorded at 330 nm for the 6-TG and fluorescence at excitation 240 nm and emission 380 nm for the BNIPDaoct. Total drug concentration was calculated per cell in respect to calibration curves.

All statistical analysis was carried out using T-Test analysis within the Microsoft Excel® software package.

Results

Synthesis and characterisation of PAA-Ox_5

PAA-Ox_5 polymers were fabricated *via* a simple substitution reaction between the primary amines in the parent PAA structure and the chloride functionality of the oxadiazole compound (Fig. 1). ^1H NMR spectroscopy was

used to identify whether polymer synthesis had been successful. The spectra (Fig.2A) showed peaks at δ0.75, δ 2.50, δ 3.00, δ1.40 and δ 1.50 which can be attributed to the CH_2 and CH groups in the homopolymer backbone, respectively. Additional peaks identified between at δ7.25-7.75 can be attributed to the aromatic CH groups present in the oxadiazole pendant group. The proton on the –SH group of the oxadiazole pendant was not observed on this spectra; this is likely to be due to rapid exchange between the thiol and D_2O solvent. FTIR analysis of the PAA-Ox_5 amphiphile was run between 4000 – 650 cm^{-1} to identify the characteristic functional groups present (Fig. 2B). Here, characteristic peaks were observed at 3350 cm^{-1} and 2800 cm^{-1} which arise from the N-H stretching and C-H stretching in the PAA backbone, respectively. Additional peaks observed at 1900 cm^{-1} and 1600 cm^{-1} indicated that hydrophobic pendant group attachment had been successful due to these peaks being attributable to the bending and stretching vibrations of the aromatic ring C=C present in the oxadiazole structure. Elemental analysis was used to quantitatively determine the degree of molar substitution of oxadiazole onto the PAA backbone. The data suggested that 5.8% grafting had occurred; which was calculated from relative sulphur content (Table 1).

Synthesis and characterisation of HNPs

Fe_3O_4 magnetic nanoparticles were successfully synthesised using a common precipitation protocol [28,47]. The polymers were subsequently electrostatically coated with PEI before gold coating. Each stage of the reaction was closely monitored using UV-Vis-NIR spectroscopy (Supplementary Data, Figure 1), photon correlation spectroscopy and zeta potential measurement (Table 1). The Fe_3O_4 nanoparticles possessed an inherent negative charge due to sulphate association attributed to the reaction pathway. After addition of the PEI onto the Fe_3O_4 surface, forming Fe_3O_4-PEI the charge increased from -17.2 mV to +50.2 mV; this large increase in surface charge is indicative of successful polymer attachment, due to the polycationic nature of PEI. After gold seeding and final coating the zeta potential dropped to +32.4 mV and +19.1 mV (Table 1) due to the electronegative charge on the colloidal gold. The final particles were visualised using TEM (Supplementary Data, Figure 2) and the particle diameter was determined to be 50 nm. Magnetic measurements were carried out using SQUID measurement. Here, the magnetization *vs.* applied field hysteresis loop was determined at 250K (Fig. 3A1). The magnetic coercivity and saturation magnetization data obtained indicate that highly crystalline Fe_3O_4 cores are present in the HNP structure which shows a high degree of order at room temperature. The zero field cooled/field cooled curve (Fig. 3A2) data shows the typical trend for ferromagnetic nanoparticles. The absence of a maximum in this data shows that the ordering temperature is above room temperature (25^oC).

Characterisation of PAA-Ox_5 and PAA-Ox_5-HNP nano-aggregates

Nano-aggregates were formed upon probe sonication of the PAA amphiphiles in deionised water. The amphiphiles were characterised using TEM, PCS and zeta potential measurement. The TEM image (Fig. 1B1) of the PAA-Ox_5 aggregates shows micellar-like structures of approximately 47 nm in diameter which is smaller than the diameter gained through PCS measurement (72 nm), however; this is due to different sample preparation and measurement techniques. The TEM measures dried samples whereas, the PCS measures the hydrodynamic radius of the aggregates suspended in water, hence obtaining a larger value. The polydispersity index (PDI) of the PAA-Ox_5 was 0.330 indicating that the nano-aggregates were not totally monodisperse. A highly positive zeta potential measurement was obtained for this amphiphile (+41.9 mV) which is unsurprising due to the amine functionality within the parent PAA backbone.

HNP conjugation was achieved through dative covalent linkage between the colloidal gold surface of the HNP and the thiol functionality in the oxadiazole pendant group of the PAA-Ox_5. It is believed that only one –SH group will be attached to one HNP due to the effects of steric hindrance coupled with the low concentration of HNPs added in the reaction. The TEM image (Fig. 1B2) indicates that attachment was successful. Here, nano-aggregate clusters are observed with small dense regions within the nano-aggregate core due to HNP attachment onto the randomly grafted oxadiazole pendants forming PAA-Ox_5-HNP. After conjugation a sharp decrease in surface charge was observed, with the zeta potential decreasing to +19.1 mV. This decrease is possibly due to the incorporation of the HNPs which may still become visible to the instrument when the aggregates are forming and disrupting under dynamic equilibrium. An increase in hydrodynamic radius (235 nm) and TEM particle diameter (175 nm) was observed which indicates that after HNP incorporation, the aggregates are no longer capable of forming compact aggregates, possibly due to steric hindrance within the hydrophobic core. Interestingly, a decrease in PDI from 0.330 (PAA-Ox_5) to 0.125 (PAA-Ox_5-HNP) occurred. This indicates that an increase in aggregate monodispersity occurs; perhaps due to the HNP hindering intramolecular aggregate formation, due to steric hindrance compared with the intermolecular aggregation of larger, less compact PAA-Ox_5-HNP aggregates. Interestingly, a clear structure was evident in the PAA-Ox_5 TEM (Fig.1B1) however, the PAA-Ox_5-HNP TEM (Fig.1B2) lacked definition. Perhaps the presence of the electron dense HNPs hinders the ability to determine accurate definition to the external polymer aggregate surfaces. The clusters of the PAA-Ox_5-HNP aggregates observed, is due to the inherent magnetic properties of the HNPs. Hence, in the drying process for the TEM the aggregates slowly aggregate towards each other before the droplet of water is completely dried. This is to be expected with any magnetic nano-material being prepared and imaged in this manner. SQUID analysis showed that the polymer construct possessed magnetic properties which further confirmed the HNP conjugation was successful (Fig. 3B). The signals obtained for M *vs.* T of the PAA-Ox_5-HNP (Fig. 3B2) were understandably much smaller than for the HNPs alone (Fig. 3A2) (10^{-12} compared with 10^{-10}); this was due to only 5% of the total mass of the amphiphile being composed of HNPs.

The CAC was determined for both amphiphiles using a hydrophobic methyl orange UV probe (Fig. 4). Here, a hypsochromic shift was observed in the λ_{max} values for absorbance in the UV spectra. The inflection point at the beginning of the curve of λ_{max} *vs.* polymer concentration is indicative of the CAC value [10]. The PAA-Ox_5 exhibited a CAC value at 0.093 $mgmL^{-1}$ which decreased to 0.049 $mgmL^{-1}$ after HNP attachment (PAA-Ox_5-HNP). This decrease in CAC value suggests that HNP addition changes the degree of hydrophobic interaction between the oxadiazole pendant groups and, hence, reduced concentrations are required for aggregate formation.

Drug loading and in vitro drug release from nano-aggregates

The model hydrophobic drugs propofol and griseofulvin were incorporated into the nano-aggregate structure *via* hydrophobic-hydrophobic interactions (Fig. 5). Polymer concentration and initial drug:polymer feed ratio were varied in order to determine the optimal drug loading parameters. Optimal drug loading for both propofol and griseofulvin was achieved at the 6 $mgmL^{-1}$ polymer concentration and 10:1 initial drug:polymer feed ratio (Supplementary data, Fig. 3). Both PAA-Ox_5 and PAA-Ox_5-HNP amphiphiles showed a polymer concentration and initial drug-feed dependant trend on drug solubilisation. Interestingly, the PAA-Ox_5-HNP nanoparticles were consistently capable of higher drug encapsulation within their hydrophobic core; this could be due to the less compact nature of the aggregates accommodating a larger quantity of drug molecules (Table 2). The

aqueous solubility of propofol was increased by 137-fold and 250-fold with the PAA-Ox_5 and PAA-Ox_5-HNP aggregates, respectively. Encapsulation efficiencies were 22.8% and 43% and drug loading capacities were 229% and 430% for PAA-Ox_5 and PAA-Ox_5-HNP, respectively. Core expansion was observed upon drug loading; TEM images showed that the aggregates increased in size from 47 nm to 200 nm, and 175 nm to 388 nm, between unloaded and drug loaded aggregates, respectively (Fig. 1B and Fig. 6A1andA2). A similar trend was observed in the hydrodynamic diameter measurements resulting from photon correlation spectroscopy (Table 1). The FTIR spectra of the freeze dried formulation (Supplementary data, Fig. 4A) showed the presence of an additional O-H peak at 3600 cm^{-1} compared with the unloaded polymers (Fig. 2B), and the *ortho*-substituted benzene ring peaks at 748 cm^{-1} were due to the substitution pattern of the functional groups present on the propofol moiety; this indicated that propofol had been successfully encapsulated in the formulation. The griseofulvin solubility studies showed that PAA-Ox_5 and PAA-Ox_5-HNP amphiphiles increased drug solubility by 53-fold and 56-fold, respectively, when compared with the intrinsic drug solubility. This resulted in 1.59 $mgmL^{-1}$ and 1.68 $mgmL^{-1}$ total drug solubilisation (Table 2). Here, the encapsulation efficiency was reduced when compared with the propofol study. However, griseofulvin is a relatively much larger molecule (molecular weight = 353 $gmol^{-1}$) compared to propofol (molecular weight = 178 $gmol^{-1}$). Similar to the propofol study, nano-aggregate core expansion was observed upon drug loading when visualised using TEM (Fig. 6A2andB2). The FTIR spectra of the griseofulvin formulations showed extra peaks at 3359 cm^{-1} (O-H), 1650 cm^{-1} (C=O), 800 cm^{-1} (substituted benzene) and a weak peak at 550 cm^{-1} (Supplementary data, Fig. 4B). These peaks correlate well with the functional groups present on the griseofulvin moiety.

The novel anticancer agent BNIPDaoct was loaded into the PAA-Ox_5 and PAA-Ox_5-HNP aggregates using the optimal parameters identified from the propofol and griseofulvin studies (Polymer concentration 6 $mgmL^{-1}$, drug: polymer feed 10:1). BNIPDaoct (molecular weight = 781 $gmol^{-1}$) is from a family of bisnaphthalimide compounds which have shown potential in cancer therapy. However, this specific analogue is hindered by its extremely hydrophobic nature, so much so in fact, that no measurable intrinsic aqueous solubility could be measured using the HPLC (coupled to a fluorescent detector) used in this study. Therefore, any increase in drug solubility is desirable. Once loaded into the respective PAA amphiphiles (PAA-Ox_5 and PAA-Ox_5-HNP), 0.84 $mgmL^{-1}$ and 0.92 $mgmL^{-1}$ drug solubilisation was achieved. These values are somewhat lower than those achieved with propofol and griseofulvin. However, worthy of note, is that BNIPDaoct is a more sterically demanding molecule and therefore less drug may be capable of being physically accommodated within the nano-aggregate core. Interestingly, the TEM images in Fig. 6A3andB3 show spherical and uniform nano-aggregates compared with the other two formulations where irregular shaped aggregates were observed. A final study was also carried out using the hydrophilic anticancer agent 6-TG. Here, the rationale was to permanently conjugate the drug molecule to the HNP incorporated into the structure of the PAA-Ox_5-HNP. Due to the hydrophilic nature of 6-TG, the mode of drug incorporation had to be achieved *via* a different mechanism to the previous studies, since no hydrophobic-hydrophobic interactions would occur (Fig. 5B). A study was carried out using the PAA-Ox_5 merely as a control. As expected, the data obtained showed an increased drug concentration present within the PAA-Ox_5-HNP core (2.8 $mgmL^{-1}$) when compared with 0.5 $mgmL^{-1}$ in the PAA-Ox_5 (Table 2); this was a 5-fold increase. The drug concentration encapsulated inside the PAA-Ox_5 is probably due to the drug molecules being dissolved in the surrounding aqueous media and not due to physical entrapment within the

hydrophobic core. The TEM images show that core expansion upon drug loading only occurred in the PAA-Ox_5-HNP and not the PAA-Ox_5 non-metallic amphiphile) (Fig. 6A4andB4).

In vitro drug release studies were carried out under '*sink conditions'* for all of the optimal formulations (Fig. 7). The studies were carried out over a period of 72 hrs. All of the hydrophobic drug formulations showed an initial 'burst' release over the first 4 hr period. Propofol was released consistently throughout the study period until 100% had been released at 72 hrs. Interestingly, the PAA amphiphiles containing the HNPs demonstrated slower drug release profiles compared with the PAA-Ox_5. Griseofulvin and BNIPDaoct release followed similar trends whereby, after the initial burst phase, a plateau was observed. Across all drugs, the PAA-Ox_5 and PAA-Ox_5-HNP formulations released 100% and 74% of drug over the 72 h study period, respectively. The BNIPDaoct-loaded aggregates however, only released 25% (PAA-Ox_5) and 18% (PAA-Ox_5-HNP) of total drug payload over the time tested, respectively. This was not a surprise, given the extremely hydrophobic nature of the drug molecule which leads to it being energetically more favourable for the drug to reside within the hydrophobic core compared to release into the aqueous phase. Interestingly, a diametric drug release profile was observed for 6-TG between the two amphiphile derivatives. That is, the PAA-Ox_5 formulation showed a 100% total drug release after 5 min. This confirms that the reported drug concentration was not, in fact, due to physical entrapment, but was due to the water-soluble drug being freely dissolved in the aqueous media. Thus, in just 5 min, drug diffusion from the formulation (in dialysis tubing) into the surrounding PBS had occurred. In contrast to this result, only 2% of 6-TG content was released from the PAA-Ox_5-HNP formulation. Since the drug incorporation was not due to hydrophobic-hydrophobic interactions but was, rather, due to permanent covalent attachment, it may appear odd that any drug was released at all. However, taking into account the small amount of 6-TG freely dissolved in the aqueous media of the formulation (and not physically attached), this result seems reasonable.

Biological characterisation of nano-aggregates and novel formulations

The cytotoxicity of the novel PAA amphiphiles on human pancreatic adenocarcinoma (BxPC-3) cells was determined using an MTT assay. The unloaded nano-aggregates were incubated with the cells for 24 hr and the total cell viability estimated compared to control wells. Upon incubation, the data showed that 50% of the total cell number was viable (IC_{50}) at 60 μgmL^{-1} (PAA-Ox_5) and 55 μgmL^{-1} (PAA-Ox_5-HNP), respectively. These similar values indicated that the incorporation of the metallic HNPs into the polymer backbone did not result in any significant increase in toxicity ($p>0.001$). MTT assays were carried out on PAA-Ox_5 and PAA-Ox_5-HNP formulations of BNIPDoact and 6-TG to determine whether the polymeric self-assemblies were capable of delivering cytotoxic drugs into the cells, thus enhancing their therapeutic effect. To determine whether the formulations enhanced the therapeutic effect of their anticancer agent, they were formulated at the polymer IC_{90} concentration (the concentration at which 90% of cells were viable). It is therefore assumed that a negligible cytotoxic effect occurs due to the polymer itself. Hence, any change in the IC_{50} value with the polymeric formulations (compared with the free drug) is as a result of an increased drug uptake or enhanced therapeutic effect. The novel formulations encapsulating BNIPDaoct were capable of a 10-fold (PAA-Ox_5) and 13-fold (PAA-Ox_5-HNP) decrease in IC_{50} value compared with the free drug (dissolved in DMSO), respectively (Fig. 8A). This data therefore indicates that the incorporation of BNIPDaoct into PAA nano-aggregates can enhance its therapeutic effect. Drug loading studies were carried out and the total drug content quantified per cell (Fig.

8B). Here, the results showed that after only 4 hr, 83-fold more drug had entered the cells in the PAA-Ox_5 compared with the free drug. Additionally, 104-fold more drug was present inside the BxPC-3 cells when incubated with the PAA-Ox_5-HNP formulation. This significant increase in cellular internalisation is probably the major contributing factor to the large decrease in cell viability and IC_{50} value after 24 hr ($p<0.001$). Interestingly, a similar trend was observed in the PAA-Ox_5-HNP formulation containing 6-TG. Here, a significant ($p<0.001$) 455-fold increase in drug uptake was observed after the 4h incubation period and a 21-fold decrease in IC_{50} was recorded. The PAA-Ox_5 formulation resulted in a 4-fold increase in cellular drug uptake and 1-fold decrease in IC_{50}, neither of which were statistically significant ($p>0.001$).

Discussion

Nanoparticulate drug delivery systems have been widely studied over the past decade. With ever-increasing knowledge and understanding, more sophisticated platforms are continually emerging – as this study demonstrates. Incorporation of HNPs into the amphiphilic polymer architecture results in bi-functional aggregates capable of simultaneous imaging and drug delivery. This study investigated the potential for incorporation of metallic HNPs into an amphiphilic graft polymer structure and the resultant physicochemical and biological effects this functionalization had. Previous work investigating HNPs as drug carriers has mainly focussed on surface conjugation of the drug to the particles [29,48]. In this study, we successfully synthesised both PAA-Ox_5 amphiphile derivatives which were characterised by elemental analysis, ^{1}H NMR and FTIR (Fig. 2). Iron oxide nanoparticles were synthesised *via* wet chemical precipitation and coated with gold using an organic intermediate (PEI). These nanoparticles were successfully incorporated into the polymer structure *via* dative covalent bonding between the gold surface and thiol functionality of the oxadiazole pendant group. TEM, zeta potential measurement and SQUID analysis confirmed the presence of the HNPs on the polymer backbone (Fig. 1B, Table 1, Fig. 3B). Nano-aggregates formed spontaneously in the aqueous environment and were characterised by PCS and TEM and their CAC determined using a hydrophobic methyl orange probe (Fig. 4). The addition of the HNPs into the intrinsic polymer structure (PAA-Ox_5-HNP) resulted in larger nano-aggregates which possessed lower CAC values (0.049 $mgmL^{-1}$) compared to the PAA-Ox_5 polymer (0.093 $mgmL^{-1}$). These values are comparable with other CAC studies using methyl orange. In 2008, Thompson and colleagues fabricated PAA amphiphiles conjugated with cholesterol, palmitoyl, cetyl and quaternary ammonium groups in 2.5-5% mole grafting ratios [6]. Here, they reported CAC values between 0.02 $mgmL^{-1}$-0.18 $mgmL^{-1}$ which were dependant on the polymer architecture [6]. In a similar study, PAA conjugated with the hydrophobic pendant groups 9-Fluorenylmethoxy carbonyl (Fmoc), Dansyl and naphtholyl (Naphth) in 5% and 10% mole grafting ratios achieved CAC values of between 0.125 -0.5 $mgmL^{-1}$ [11]. Our cytotoxicity studies of the PAA derivatives indicated IC_{50} values of 60 μgmL^{-1} and 55 μgmL^{-1} for PAA-Ox_5 and PAA-Ox_5-HNP, respectively (Fig. 8A). Here, the IC_{50} values for both amphiphiles are not significantly different ($p>0.001$). This work follows the extensive investigations into the stability and toxicity of HNPs in BxPC-3 cells that have been reported recently [29]. This study showed that over a 2 week period the HNPs appeared to be chemically stabile in physiological media (pH 4.6 and 7.2). No significant cell viability reduction was observed in the BxPC-3 cells after 1 week incubation up to 100 μgmL^{-1}. In addition, negligible cell membrane damage or free radical production was detected after 72 h incubations up to 25 μgmL^{-1} [29].

Drug incorporation into the nano-aggregates was achieved by two mechanisms. Firstly, hydrophobic drug molecules are encapsulated within the hydrophobic core of the aggregates due to the preferential reduction in Gibbs' free energy (Fig. 5A). Here, two model hydrophobic drugs, propofol and griseofulvin were used in order to investigate the optimal parameters, which included the polymer concentration and initial drug: polymer mass feed ratio for drug encapsulation to occur. Using the optimal formulation conditions identified in these studies (6 $mgmL^{-1}$ polymer concentration and 10:1 initial drug:polymer feed ratio), an additional hydrophobic drug (BNIPDaoct) was investigated and incorporated into the core of the PAA amphiphiles in a similar manner (Supplementary data, Figure 3). Our drug solubilisation results were in agreement with previous studies on the drug loading of PAA amphiphiles [13]. Further, the PAA derivatives tested proved to be universal drug solubilizers for a range of hydrophobic drugs. The maximum solubilisation concentrations were recorded as 25.79 $mgmL^{-1}$, 1.68 $mgmL^{-1}$ and 0.92 $mgmL^{-1}$ for propofol, griseofulvin and BNIPDaoct, respectively (Table 2). Interestingly, these loading maxima were all achieved with the PAA-Ox_5-HNP amphiphile. Perhaps, the less compacted core resulted in greater core expansion and thus drug accommodation resulting in greater drug loading and encapsulation efficiencies (Table 2). Previous studies using PAA amphiphiles with Dansyl pendant groups (with 10% mole grafting) reported maximum drug solubilisation of 22.4 $mgmL^{-1}$ and 16.71 $mgmL^{-1}$ for propofol and griseofulvin, respectively [13]. Here, the propofol results are comparable to ours at lower molar pendant grafting levels (5%) with the oxadiazole group, however, our griseofulvin solubilisation results are notably lower. The reason for this is not clear, although it could be due to the increased core expansion upon drug loading resulting in larger aggregates which were then removed during the filtering process. Other studies reported cholesterol modified PAA (Ch5) for BNIPDaoct solubilisation achieved 0.3 $mgmL^{-1}$ drug encapsulation with 1 $mgmL^{-1}$ polymer concentration, 5% mole cholesterol grafting and a 1:1 initial drug:polymer mass feed ratio [49]. Here, the PAA-Ox5-HNP formulation achieved a greater drug loading (0.9 $mgmL^{-1}$) but with a lower % loading capacity (15% compared to the 30%) to the Ch5-BNIPDaoct formulation.

The second mechanism of drug incorporation concerned the conjugation of the model hydrophilic drug 6-TG onto PAA-Ox_5-HNP amphiphile (*via* the HNP) (Fig. 5B). This was achieved through dative covalent linkage between the colloidal gold surface and the thiol moiety in the 6-TG structure. 6-TG is a freely water-soluble drug and therefore encapsulation *via* hydrophobic-hydrophobic interaction should not occur; hence, PAA-Ox_5 was used as a control vehicle. The conjugation of 6-TG onto the PAA-Ox_5-HNP structure could possibly protect the drug on its journey to target site and reduce undesirable side effects. Here, the data showed an exciting solubility increase to 2.8 $mgmL^{-1}$ with PAA-Ox_5-HNP compared with 0.5 $mgmL^{-1}$ with PAA-Ox_5. This indicates that the drug had successfully incorporated into the HNP-amphiphile structure which was also confirmed with an increase in nano-aggregate diameter using TEM (Fig. 6B4).

Biological investigations into the BNIPDaoct and 6-TG formulations showed consistently that greater cell uptake occurred after 4 h incubation with BxPC-3 cells compared with free drug. This exciting finding is in agreement with other studies which have shown that drugs either encapsulated or physically conjugated onto nanoparticulates experience enhanced cellular uptake [50]. Other work in BxPC-3 cells investigated the cellular response to 6-TG after its conjugation to the HNPs onto HNP surface showed enhanced cellular uptake of the conjugated 6-TG when compared with free drug with a resulting 10-fold decrease in IC_{50} [29]. At these drug concentrations the polymer level is below its CAC. However, the added hydrophobicity of the drug molecule into the intrinsic structure of the nano-aggregate may be enough to stabilize the system. Little is known in this

area as previous studies have observed that even at polymer concentrations below IC_{50} *in vivo* enhancement in drug efficacy occurs [49]. These *in vitro* studies can only be classed as indicators for *in vivo* situations and further in vivo studies must be carried out to truly deduce the clinical efficacy. Further, it has been well documented that nanoparticulates preferentially accumulate inside the leaky vasculature of rapidly proliferating tumour sites which is an example of a passive targeting approach. Hence, this technology could enhance current chemotherapeutic strategies by penetrating further into the dense stroma surrounding tumour sites particularly in pancreatic cancer.

Conclusion

Novel PAA-Ox_5-HNPs have been successfully synthesised and have demonstrated good potential as drug solubilizers / carriers. Our results indicate that after conjugation of metallic HNPs onto the polymer amphiphile structure, drug loading is increased with an accompanying decrease in the *in vitro* drug release rate. *In vitro* biological studies have shown that these novel PAA amphiphile formulations are capable of enhancing the efficacy of cancer therapeutics over the free drug. Moving forward, *in vivo* studies should be carried out in order to further elucidate the potential of these polymer constructs for image guided drug delivery.

Acknowledgement

This work was funded by the Institute of Science and Technology in Medicine and the School of Pharmacy, Keele University. The NMR and ICP-OES analysis was carried out in the Lennard-Jones Laboratories in the School of Physical and Geographical Sciences. The magnetometer used in this research was obtained through the Science City Advanced Materials project: Creating and Characterizing Next Generation Advanced Materials project, with support from Advantage West Midlands (AWM) and part funded by the European Regional Development Fund (ERDF).

Conflict of Interest

The authors declare they have no conflict of interest in this work.

References

1. Bromberg L. Polymeric micelles in oral chemotherapy. J Control Release 2008; 128: 99-112.
2. Kwon G, Okano T. Polymeric micelles as new drug carriers. Adv Drug Deliver Rev 1996; 21: 107-116.
3. Branco MC, Schneider JP. Self-assembling materials for therapeutic delivery. Acta Biomater 2009; 5: 817-813.
4. Qui L, Zheng C, Jin Y, Zhu K. Polymeric micelles as nanocarriers for drug delivery. Expert Opin Ther Pat 2007; 17: 819-30.
5. Letchford K, Burt H. A Review of the formation and classification of amphiphilic block copolymer nanoparticulate structures: micelles, nanospheres, nanocapsules and polymersomes. Eur J Pharm Biopharm 2007; 65: 259-269.
6. Thompson C, Ding C, Qu X, *et al*. The effect of polymer architecture on the nano self-assemblies based on novel comb-shaped amphiphilic poly(allylamine). Colloid Polym Sci 2008: 286: 1511-1526.
7. Lapienis G. Star-shaped polymers having PEO arms. Prog Polym Sci 2009; 34: 852- 892.
8. Duncan R, Izzo L. Dendrimer biocompatability and toxicity. Adv Drug Deliver Rev 2005; 57: 2215-2237.
9. Hoskins C, Kong Thoo Lin P, Cheng WP. A review on comb-shaped amphiphilic polymers for hydrophobic drug solubilization. Ther Deliver 2012; 3: 59-79.
10. Cheng WP, Gray AI, Tetley L, *et al.* Polyelectrolyte Nanoparticles with High Drug Loading Enhance the Oral Uptake of Hydrophobic Compounds. Biomacromolecules 2006; 7: 1509-1520.

11. Hoskins C, Kong Thoo Lin P, Tetley L, Cheng WP. Novel fluorescent amphiphilic poly(allylamine) and their supramolecular self-assemblies in aqueous media. Polym Advan Technol 2011: 23: 710-719.
12. Uchegbu IF, Schältzen AG, Tetley L. Polymeric chitosan based vesicles for drug delivery. J Pharmaceut Pharmacol 1998; 50: 453-458.
13. Hoskins C, Kong Thoo Lin P, Tetley L, Cheng WP. The use of nano polymeric self-assemblies based on novel amphiphilic polymers for oral hydrophobic drug delivery. Pharm Res 2012; 3: 59-79.
14. Shubayev VI, Pisanic TR, Jin S. Magnetic nanoparticles for theragnostics. Adv Drug Deliver Rev 2009; 61: 467-477.
15. McCarthy JR, Weissleder R. Multifunctional magnetic nanoparticles for targeted imaging and therapy. Adv Drug Deliver Rev 2008; 60: 1241-1251.
16. Bulte JWM, Douglas T, Witwer B, *et al.* Magnetodendrimers allow endosomal magnetic labeling and in vivo tracking of stem cells. Nature Biotechnol 2001; 19: 1141-1147.
17. Xu P, Zeng GM, Huang DL, *et al.* Use of iron oxide nanomaterials in wastewater treatment: A review. Sci Total Environ 2012; 424: 1-10.
18. Freund H-J. Clusters and islands on oxides: from catalysis via electronics and magnetism to optics. Surface Science 2002; 500: 271-299.
19. Arruebo M, Fernádez-Pacheco R, Velasco B, *et al.* Antibody-Functionalized Hybrid Superparamagnetic Nanoparticles. Adv Funct Mater 2007; 17: 1473-1479.
20. Hoskins C, Wang L, Cuscheiri A. Dilemmas in the reliable estimation of the in-vitro cell viability in magnetic nanoparticle engineering: which tests and what protocols? Nanoscale Res Lett 2012; 7: 77.
21. Hoskins C, Cuschieri A, Wang L. The cytotoxicity of polycationic iron oxide nanoparticles: Common endpoint assays and alternative approaches for improved understanding of cellular response mechanism. Int J Nanobiotech 2012; 10: 15.
22. Drugs.com. Drug Information Online: Feridex [Online] [2008] [cited 2013] Available at: http://www.drugs.com/pro/feridex.html
23. Jain TK, Reddy MK, Morales MA, *et al.* Biodistribution, Clearance and Biocompatibility of Iron Oxide Magnetic Nanoparticles in Rats. Mol Pharm 2007; 5: 316-327.
24. Minotti G, Aust SD. The requirement for iron (III) in the initiation of lipid peroxidation by iron (II) and hydrogen peroxide. J Biol Chem 1987; 262: 1098-1104.
25. Goon IY, Lai LMH, Lim M, *et al.* Fabrication and dispersion of gold-shell protected magnetite nanoparticles: Systematic control using polyethylenimine. Chem Mater 2009; 21: 673-681.
26. Huang C, Jiang J, Muangphat C, Sun X, Hao Y. Trapping iron oxide into hollow gold nanoparticles. Nanoscale Res Lett 2011; 6: 1-5.
27. Jain PK, El-Sayed IH, El-Sayed MA. Au nanoparticles target cancer. Nanotoday 2007; 2: 18-29.
28. Barnett CM, Gueorguieva M, Lees MR, *et al.* Effect of the hybrid composition on the physicochemical properties and morphology of iron oxide–gold nanoparticles. J Nanoparticle Res 2012; 14: 1170.
29. Barnett CM, Gueorguieva M, Lees MR, McGarvey D, Hoskins C. Physical stability, biocompatibility and potential use of hybrid iron oxide-gold nanoparticles as drug carriers. 2013; *Under review*
30. Ravenelle F, Gori S, Le Garrec D, *et al.* Novel Lipid and Preservative-free Propofol Formulation: Properties and Pharmacodynamics. Pharm Res 2008; 25: 313-319.
31. Gelderblom H, Verweij J, Nooter K, Sparreboom A. Cremophor EL: the drawbacks and advantages of vehicle selection for drug formulation. Eur J Cancer 2001; 37: 1590-1598.
32. Baker MT, Naguib M. Propofol: The Challenges of Formulation. Anesthesiology 2005; 103: 860-876.
33. Lundström S, Zachrisson U, Fürst CJ. When Nothing Helps: Propofol as Sedative and Antiemetic in Palliative Cancer Care. J Pain Symptom Manag 2005; 30: 570-577.
34. Zili Z, Sfar S , Fessi H. Preparation and characterization of poly-ε-caprolactone Nanoparticles containing griseofulvin. Int J Pharm 2005; 294: 261-267.
35. Trotta M, Gallarate M, Carlotti ME, Morel S. Preparation of griseofulvin Nanoparticles from water-dilutable microemulsions. Int J Pharm 2003; 254: 235-242.
36. Tur KM, Ch'ng H-S, Baie S. Use of bioadhesive polymer to improve the bioavailability of griseofulvin. Int J Pharm 1997; 148: 63-71.
37. Dahan A, Hoffman A. The effect of different lipid based formulations on the oral adsorption of lipophilic drugs: The ability of in vitro lipolysis and consecutive ex vivo intestinal permeability data to predict in vivo bioavailability. Eur J Pharm Biopharm 2007: 67: 96-105.
38. Fujioka Y, Metsugi Y, Ogawara K-I, Higaki K, Kimura T. Evaluation of in vivo dissolution behaviour and GI transit of griseofulvin, a BSC class II drug. Int J Pharm 2008; 352: 36-43.
39. Finkelstein E, Amichai B, Grunwald MH. Griseofulvin and its uses. Int J Antimicrob Ag 1996; 6: 189-194.

40. Ahmed IS, Aboul-Einien MH, Mohamed OH, Farid SF. Relative bioavailability of griseofulvin lyophilized dry emulsion tablet *vs.* immediate release tablet: A single-dose, randomized, open-label, six-period, crossover study in healthy adult volunteers in the fasted and fed states. Eur J Pharm Sci 2008; 35: 219-225.
41. Oliveira J, Ralton L, Tavares J, *et al.* The synthesis and the in vitro cytotoxicity studies of bisnaphthalimidoproply polyamine derivatives against colon cancer cells and parasite Leishmania infantum. Bioorgan Med Chem 2007; 15: 541-545.
42. Braña MF, Cacho M, Gradillas A, de Pascual-Teresa B, Ramos A. Intercalators as Anticancer Drugs. Curr Pharm Design 2007; 7: 1754-1780.
43. Braña MF, Castellano JM, Morán M, *et al.* Bis-naphthalimides. 2. Synthesis and biological activity of 5,6-acenaphthalimidoalkyl-1,8-naphthalimidoalkyl amines. Eur J Med Chem 1995; 30: 235-239.
44. Lancaster DL, Patel N, Lennard L, Lilleyman JS. 6-Thioguanine in children with acute lymphoblastic leukaemia: influence of food on parent drug pharmacokinetics and 6-thioguanine nucleotide concentrations. BJCP 2001; 56: 531-539.
45. Katsanos K, Tsianos EV. Non-TPMT determiniants of azathioprine toxicity in imflammatory bowel disease. Ann Gastroent 2010; 23: 95-101.
46. Uchegbu IF, Sadiq L, Arastoo M, *et al.* Quaternary ammonium palmitoyl glycol chitosan – a new polysoap for drug delivery. Int J Pharm 2001; 224: 185-199.
47. Andrés Vergés M, Costo R, Roca AG, *et al.* Uniform and water stable magnetite nanoparticles with diameters around the monodomain-multidomain limit. J Phys D Appl Phys 2008; 41:13.
48. Wagstaff AJ, Brown SD, Holden MR, *et al.* Cisplatin drug delivery using gold-coated iron oxide nanoparticles for enhanced tumour targeting with external magnetic fields. Inorg Chim Acta 2012; 393:328-333.
49. Hoskins C, Ouaissi M, Lima SC, *et al.* In vitro and in vivo anticancer activity of a novel nano-sized formulation based on self-assembling polymers against pancreatic cancer. Pharm Res 2010; 27: 2694-2703.
50. Nishiyama N, Kataoka K. Current state, achievements, and future prospects of polymeric micelles as nanocarriers for drug and gene delivery. Pharmacol Therapeut 2006; 112: 630-648.

Figures

Figure 1. A) Chemical synthesis of PAA-Ox_5 and PAA-Ox_5-HNP and B) TEM images of 1) PAA-Ox_5 and 2) PAA-Ox_5-HNP nano-aggregates.

Figure 2. Chemical characterisation of PAA-Ox5. A) ^{1}H NMR spectra in D_2O carried out on a 400MHz NMR at 25^{o}C and B) FTIR spectra run on a diamond tipped ATR-FTIR (64 scans).

Figure 3. Magnetization data of A)HNPs and B) PAA-Ox_5-HNP. 1) M(T) curves measured in zero-field cooled warming and field-cooling mode, 2) M(H) curves collected at 250 K between -4 and 4 MA/m.

Figure 4. CAC measurement of nano-aggregates using hydrophobic methyl orange probe resulting in a hypsochromic shift upon aggregate formation. Samples measured via UV-Vis spectroscopy (n=3, ±SD).

Figure 5. Mechanism of A) hydrophobic drug molecule encapsulation and B) 6-TG conjugation to PAA-Ox_5-HNP via dative covalent bonding between the thiol and gold surface of the HNP.

Figure 6. TEM images of optimal formulations of A) PAA-Ox_5 and B) PAA-Ox_5-HNP nano-aggregates incorporating 1) propofol, 2) griseofulvin, 3) 6-TG and 4) BNIPDaoct.

Figure 7. Drug release from optimal formulations over 72 h. Study carried out in PBS under 'sink' conditions at 37 °C with constant stirring (n=3, ±SD).

Figure 8. Biological investigation on BxPC-3 cells. A) Cytotoxicity evaluation of polymers and formulations and B) cellular uptake of 6-TG and BNIPDaoct (n=3, ±SD). * denotes level of significance increase in IC_{50} between free drug and formulation ($p<0.001$). ** denotes level of significance increase in drug uptake between free drug and formulation ($p<0.001$).

Tables

Table 1. Physicochemical analysis of PAA, PAA-Ox_5 nano-aggregates, HNPs, PAA-Ox_5-HNP nano-aggregates and optimal drug loading formulations.

Table 2. Drug loading of PAA amphiphiles with hydrophobic and hydrophilic drug molecules via hydrophobic interaction and direct conjugation, respectively (n=3, ±SD).

Figures

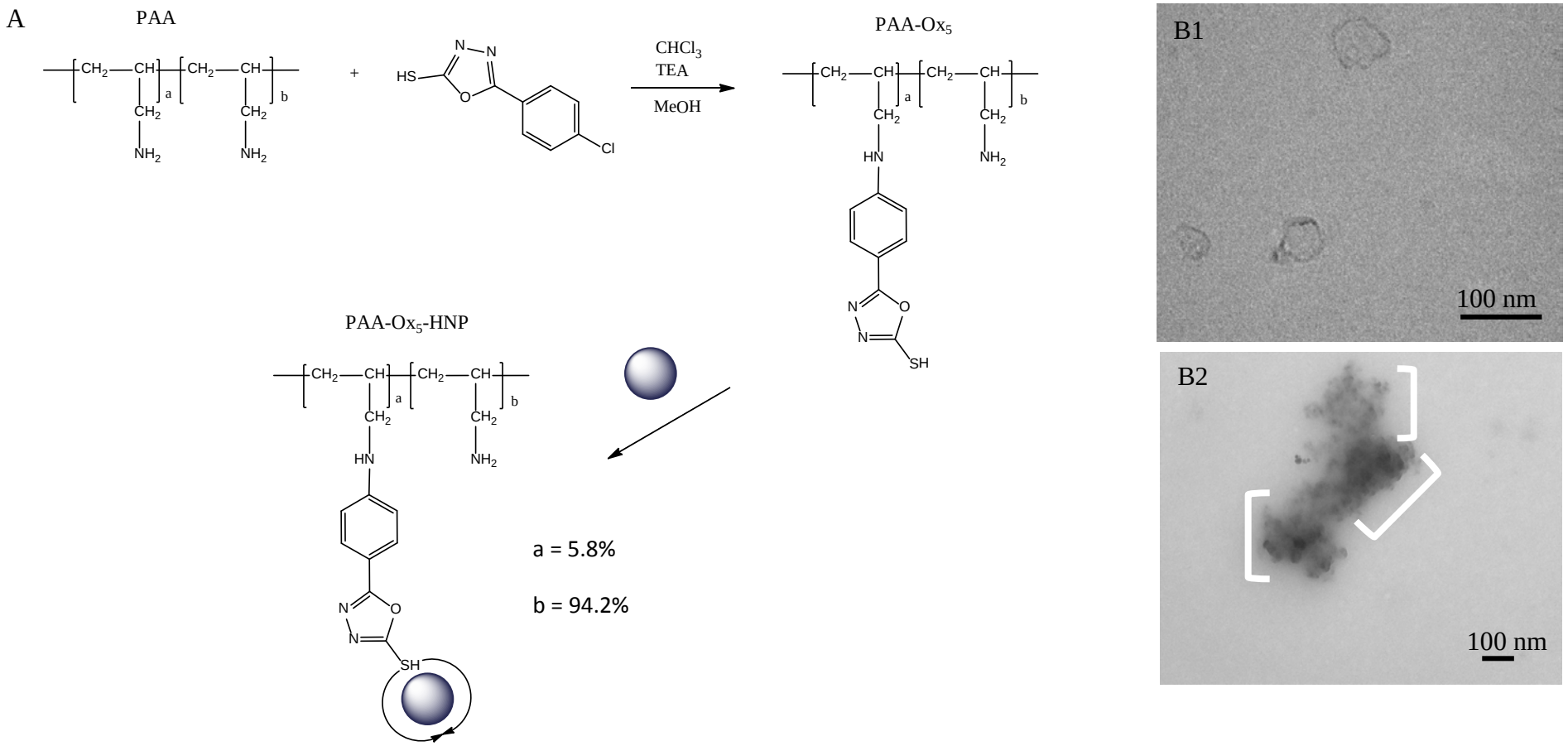

Figure 1. A) Chemical synthesis of PAA-Ox_5 and PAA-Ox_5-HNP and B) TEM images of 1) PAA-Ox_5 and 2) PAA-Ox_5-HNP nano-aggregates.

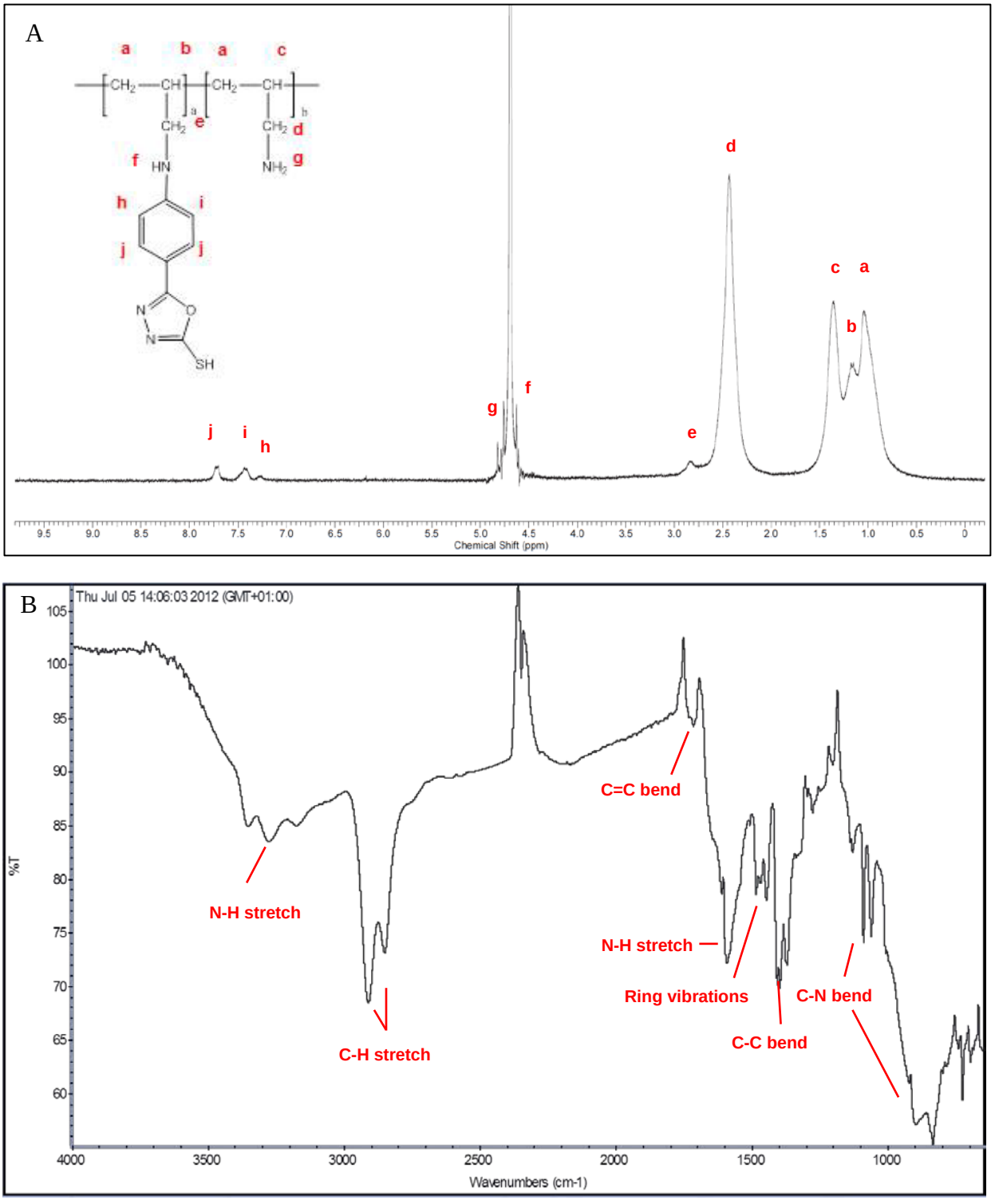

Figure 2. Chemical characterisation of PAA-Ox5. A) ^{1}H NMR spectra in D_2O carried out on a 400MHz NMR at 25°C and B) FTIR spectra run on a diamond tipped ATR-FTIR (64 scans).

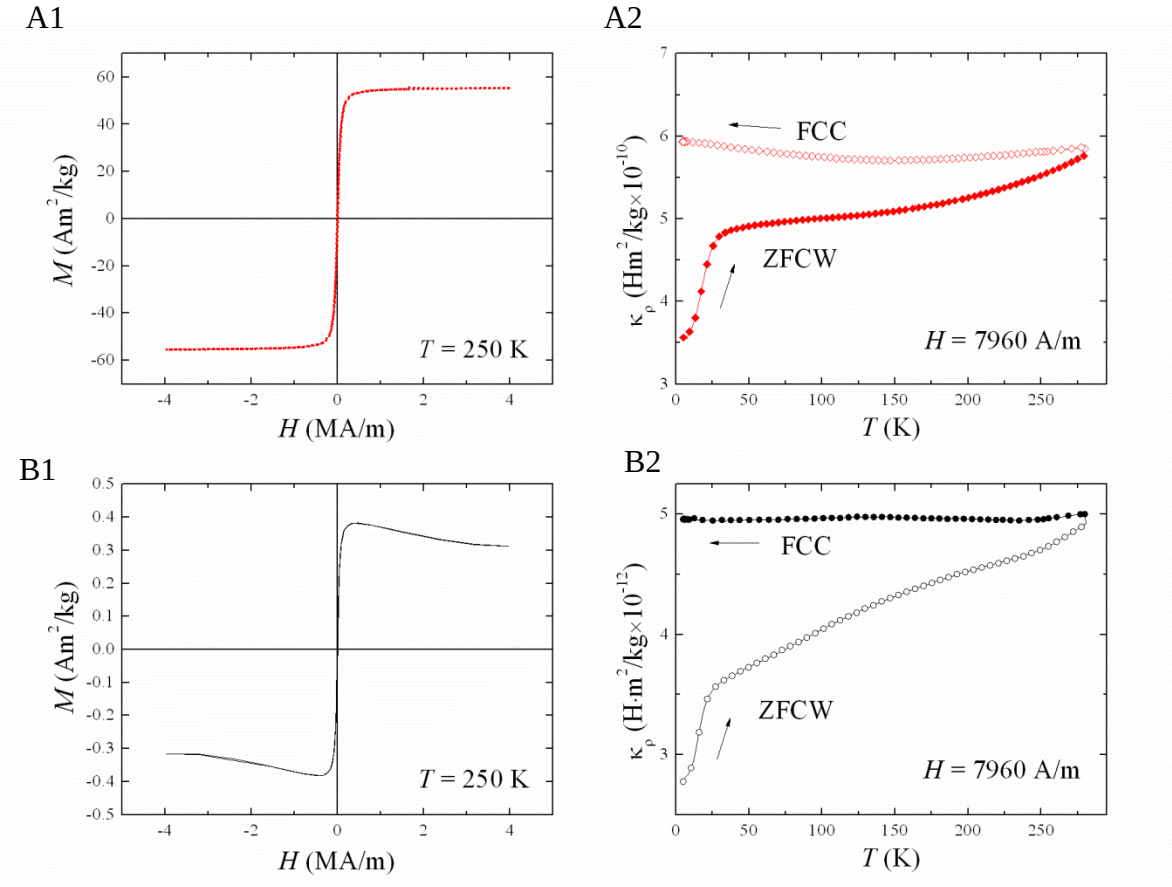

Figure 3. Magnetization data of A)HNPs and B) PAA-Ox_5-HNP. 1) M(T) curves measured in zero-field cooled warming and field-cooling mode, 2) M(H) curves collected at 250 K between -4 and 4 MA/m.

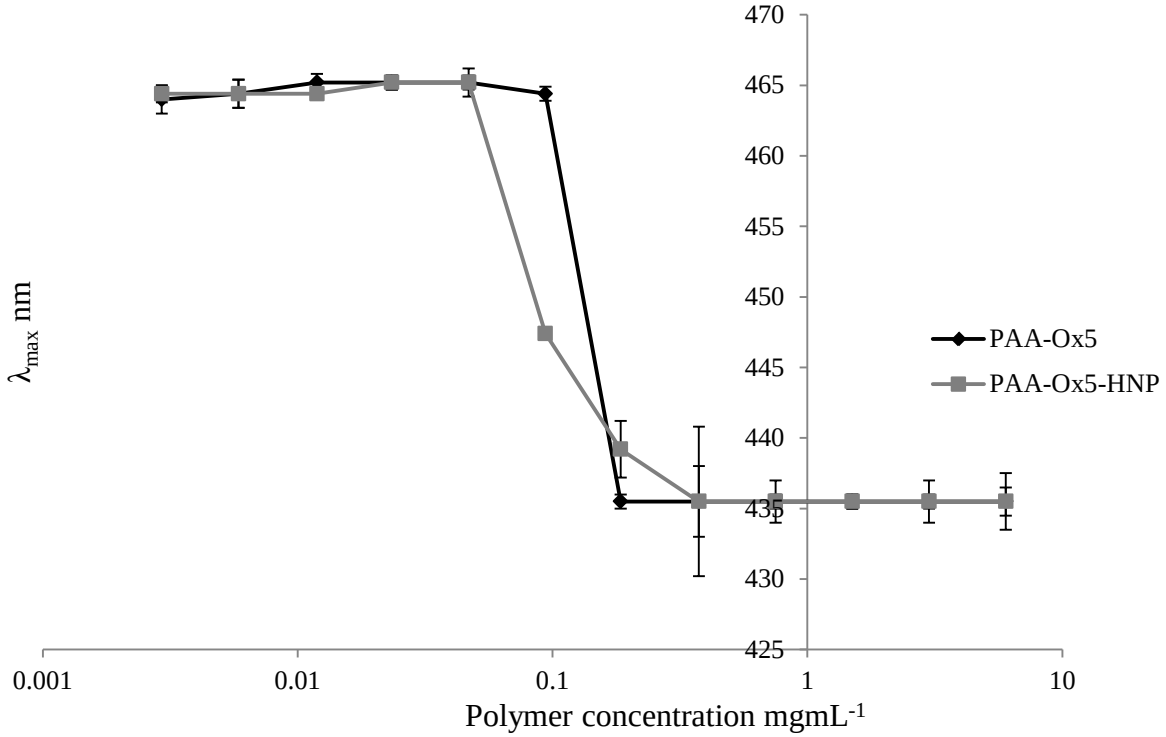

Figure 4. CAC measurement of nano-aggregates using hydrophobic methyl orange probe resulting in a hypsochromic shift upon aggregate formation. Samples measured via UV-Vis spectroscopy (n=3, ±SD).

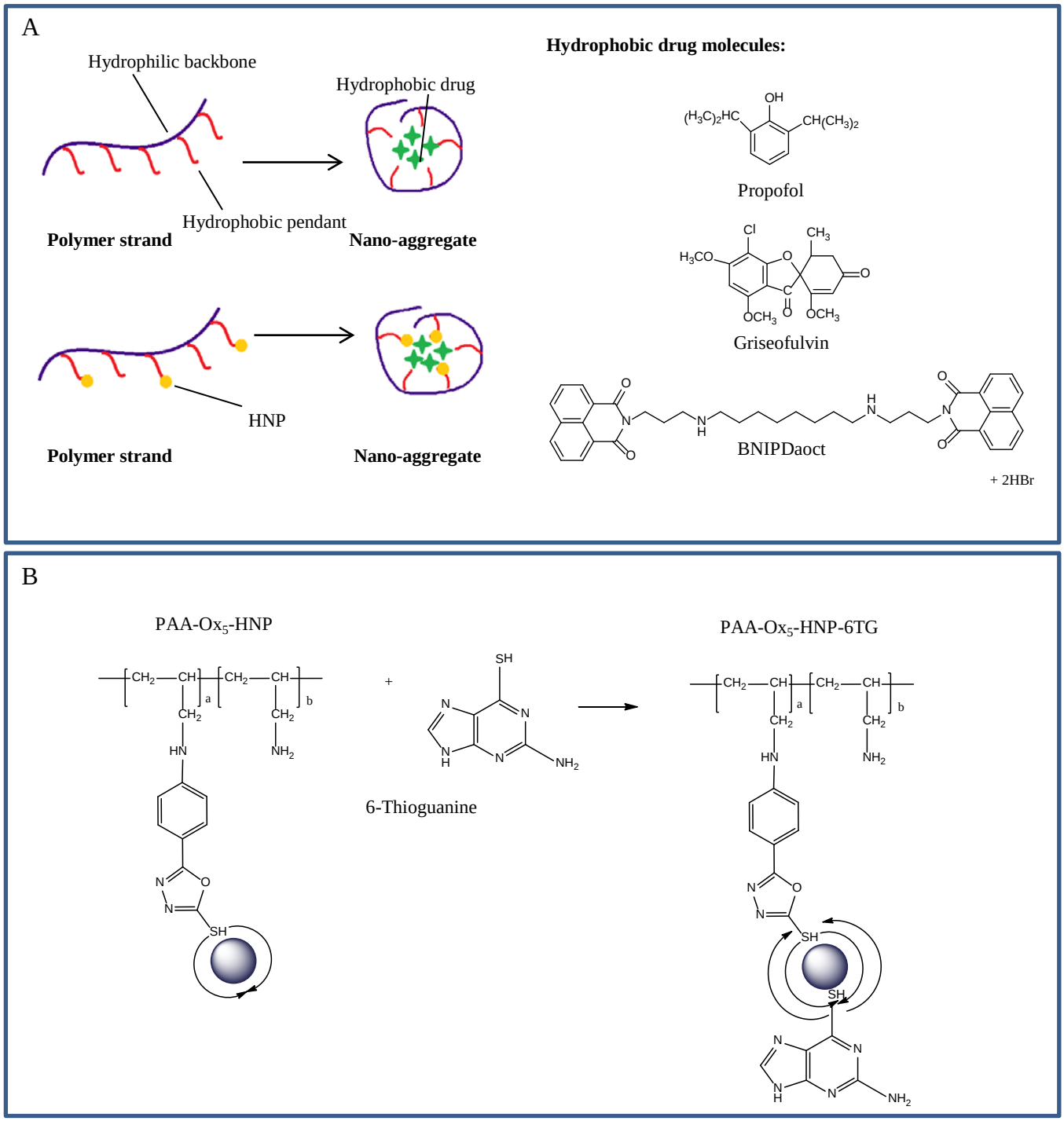

Figure 5. Mechanism of A) hydrophobic drug molecule encapsulation and B) 6-TG conjugation to PAA-Ox_5-HNP via dative covalent bonding between the thiol and gold surface of the HNP.

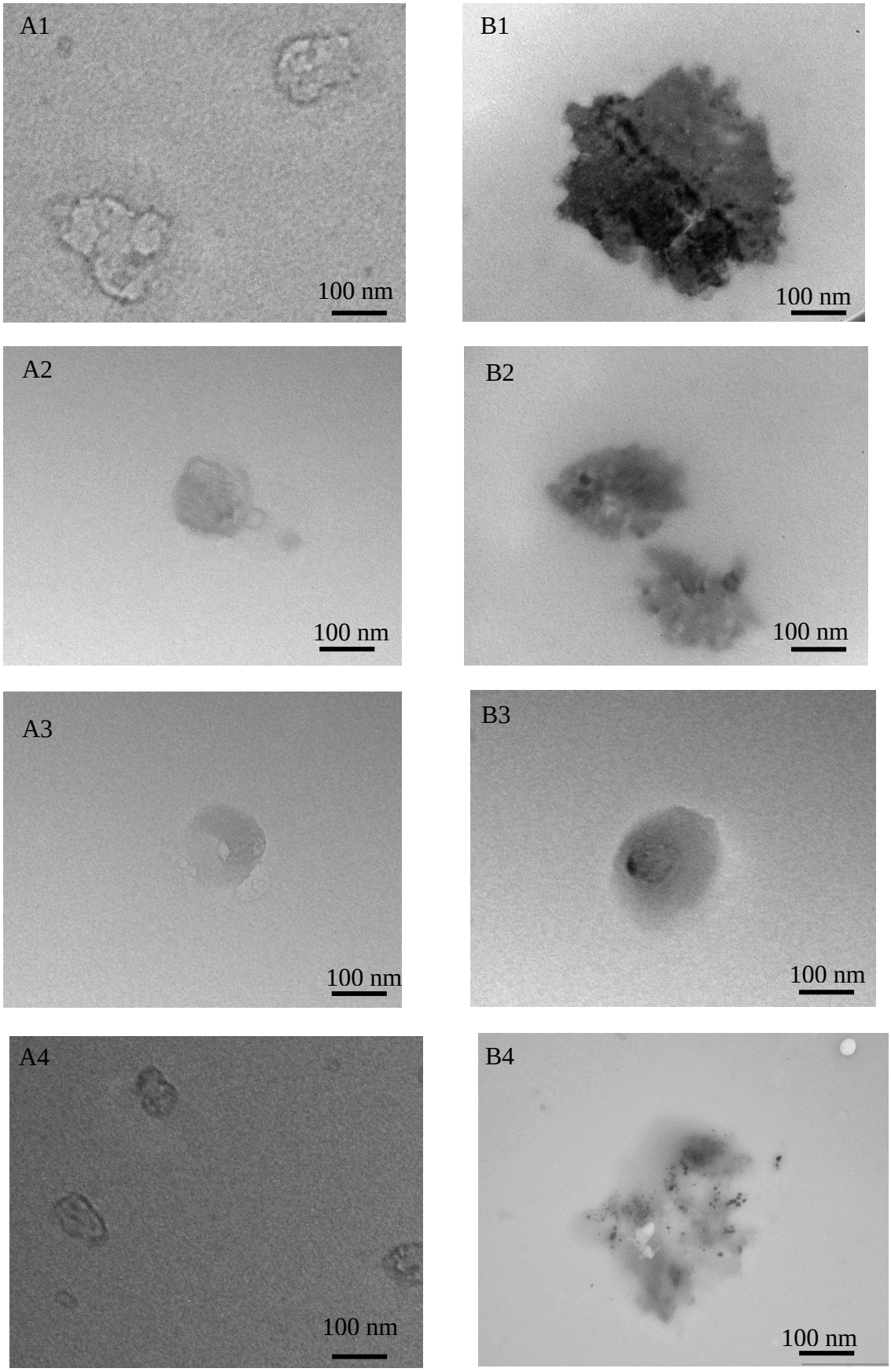

Figure 6. TEM images of optimal formulations of A) PAA-Ox_5 and B) PAA-Ox_5-HNP nano-aggregates incorporating 1) propofol, 2) griseofulvin, 3) 6-TG and 4) BNIPDaoct.

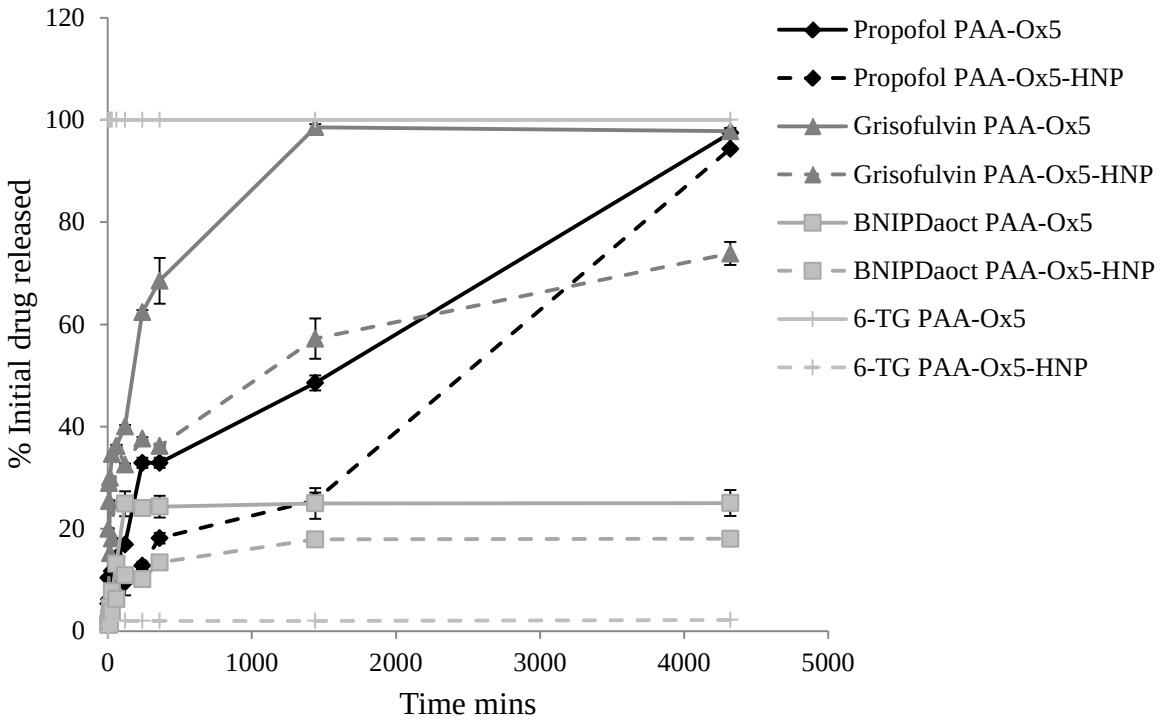

Figure 7. Drug release from optimal formulations over 72 h. Study carried out in PBS under 'sink' conditions at 37 °C with constant stirring (n=3, ±SD).

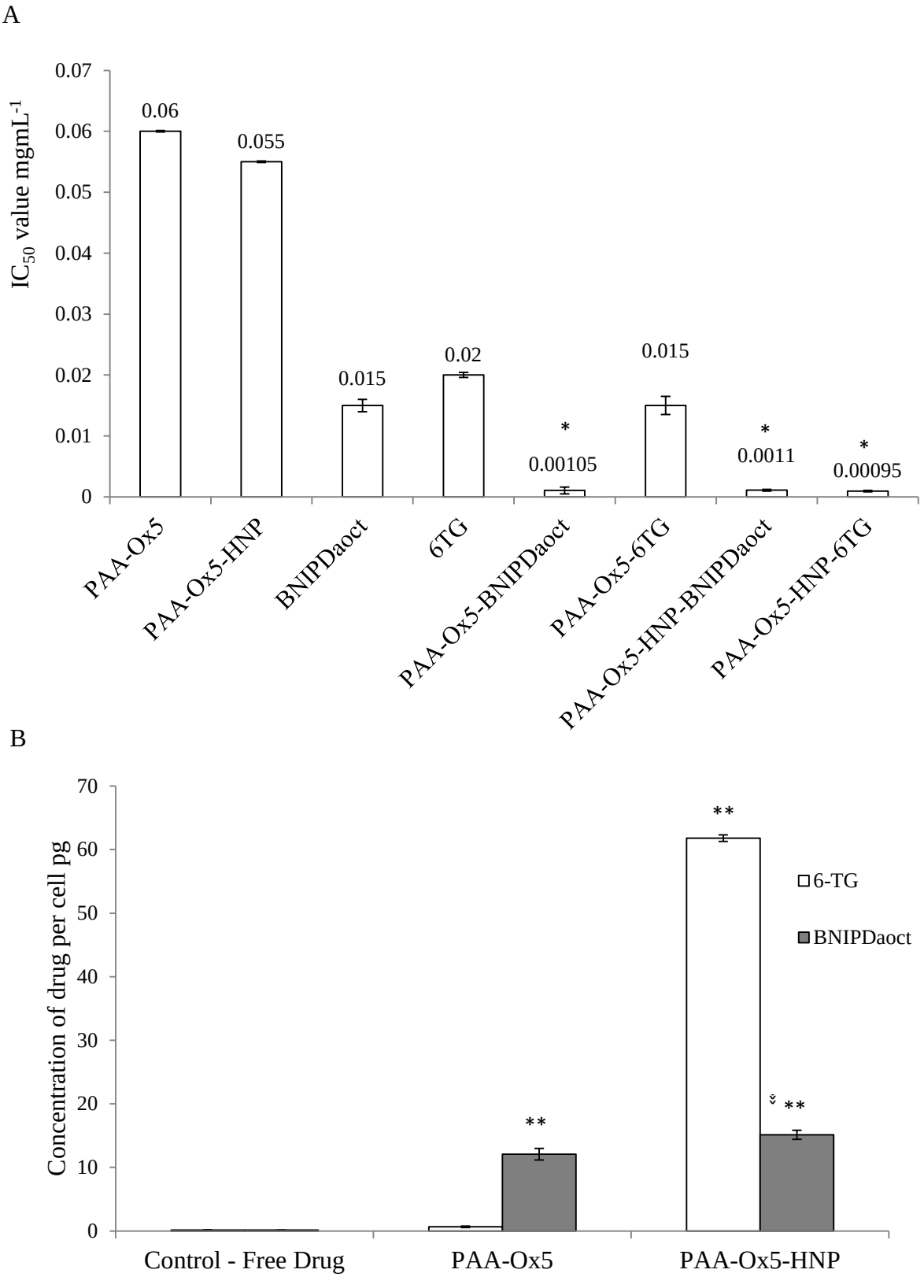

Figure 8. Biological investigation on BxPC-3 cells. A) Cytotoxicity evaluation of polymers and formulations and B) cellular uptake of 6-TG and BNIPDaoct (n=3, ±SD). * denotes level of significance increase in IC_{50} between free drug and formulation ($p<0.001$). ** denotes level of significance increase in drug uptake between free drug and formulation ($p<0.001$).

Table 1. Physicochemical analysis of PAA, PAA-Ox_5 nano-aggregates, HNPs, PAA-Ox_5-HNP nano-aggregates and optimal drug loading formulations.

Particle	**Molar grafting level of PAA amphiphiles (monomer:pendant)**	**Metal content analysis µgmL^{-1}**		**Size nm (±SD) from TEM**	**Size nm (±SD) from PCS**	**PDI (±SD)**	**Zeta potential mV (±SD)**
		Fe	**Au**				
PAA	1:0.000	-	-	-	-	-	-
PAA-Ox_5	1:0.058	-	-	47 (0.5)	72 (0.680)	0.330 (0.026)	+41.9 (3.282)
Fe_3O_4	-	5215	-	50 (0.5)	2159 (154.0)	0.675 (0.012)	-17.2 (1.000)
Fe_3O_4-PEI	-	2651	-	55 (1.0)	208 (7.125)	0.321 (0.012)	+50.2 (3.052)
Fe_3O_4-PEI-Au_{SEED}	-	1002	59	60 (0.5)	201 (12.245)	0.372 (0.004)	+32.4 (2.001)
Fe_3O_4-PEI-Au_{COAT} (HNP)	-	852	218	70 (0.5)	124 (12.221)	0.114 (0.002)	+12.2 (1.051)
PAA-Ox_5-HNP	1:0.058	50	7	175 (1.5)	235 (2.152)	0.125 (0.012)	+19.1 (1.498)
PAA-Ox_5-Propofol	1:0.058	-	-	200 (2.5)	514 (3.215)	0.463 (0.178)	+48.4 (3.792)
PAA-Ox_5-HNP-Propofol	1:0.058	50	7	388 (5.0)	526 (2.541)	0.237 (0.014)	+39.1 (3.064)
PAA-Ox_5-Griseofulvin	1:0.058	-	-	133 (0.5)	162 (2.702)	0.151 (0.005)	+25.0 (3.276)
PAA-Ox_5-HNP-Griseofulvin	1:0.058	50	7	200 (0.5)	261 (0.798)	0.814 (0.072)	+31.6 (2.479)
PAA-Ox_5-BNIPDaoct	1:0.058	-	-	167 (3.5)	109 (2.554)	0.341 (0.069)	+35.5 (2.783)
PAA-Ox_5-HNP-BNIPDaoct	1:0.058	50	7	222 (1.5)	206 (4.771)	0.222 (0.019)	+14.3 (1.118)
PAA-Ox_5-6TG	1:0.058	-	-	55 (1.0)	157 (3.045)	0.175 (0.010)	+38.9 (3.051)
PAA-Ox_5-HNP-6TG	1:0.058	50	7	250 (1.5)	313 (2.352)	0.455 (0.003)	+33.9 (2.659

Table 2. Drug loading of PAA amphiphiles with hydrophobic and hydrophilic drug molecules via hydrophobic interaction and direct conjugation, respectively (n=3, ±SD).

Polymer	**Polymer concentration mgmL^{-1}**	**Drug**	**Incorporation mechanism**	**Initial drug feed: polymer ratio**	**Maximum drug loading concentration mgmL^{-1} (n=3, ±SD)**	**Increment increase from aqueous solubility (- fold)**	**Excipient: Drug ratio**	**% EE**	**%LC**
PAA-Ox$_5$	6	Propofol	Electrostatic	10:1	13.71 (0.013)	137	0.44	22.8	229
	6	Griseofulvin	Electrostatic	10:1	1.59 (0.002)	53	3.78	2.7	27
	6	BNIPDaoct	Electrostatic	10:1	0.84 (0.102)	-	7.14	1.4	14
	6	6-TG	Conjugation	10:1	0.5 (0.012)	-	12	0.8	8.3
PAA-Ox$_5$-HNP	6	Propofol	Electrostatic	10:1	25.79 (0.035)	250	0.23	43	430
	6	Griseofulvin	Electrostatic	10:1	1.68 (0.064)	56	3.57	2.8	28
	6	BNIPDaoct	Electrostatic	10:1	0.92 (0.111)	-	6.52	1.5	15
	6	6-TG	Conjugation	10:1	2.8 (0.102)	-	2.14	4.7	47